



# The 16-year periodicity in the winter surface temperature variations in the Antarctic Peninsula region

Oleksandr Evtushevsky<sup>1</sup> · Asen Grytsai<sup>1</sup> · Oleksiy Agapitov<sup>1,2</sup> · Volodymyr Kravchenko<sup>1</sup> · Gennadi Milinevsky<sup>1,3,4</sup>

Received: 7 December 2020 / Accepted: 8 July 2021 / Published online: 16 July 2021  
© The Author(s), under exclusive licence to Springer-Verlag GmbH Germany, part of Springer Nature 2021

## Abstract

The aim of this work is a comprehensive study of the 16-year periodicity of winter surface temperature in the Antarctic Peninsula (AP) region, described earlier, and its possible source based on weather station records over the 1952–2019 period making use of the Scientific Committee on Antarctic Research (SCAR) Reference Antarctic Data for Environmental Research (READER) database, as well as Fourier and wavelet analysis methods. It is shown that interdecadal oscillation with a period of about 16 years dominates in the northern AP (Esperanza and Orcadas), which is consistent with previous results. The 16-year periodicity is found to closely correlate with the sea level pressure anomaly in the southwestern Atlantic associated with the zonal wave-3 and the Southern Annular Mode patterns. The correlation maximum in the southwestern Atlantic, having the characteristic features of the anticyclonic circulation, affects the surface temperature in the northern AP through the related structure of the zonal and meridional wind anomalies. This effect is weaker to the south, where the Vernadsky station data do not show a regular interdecadal periodicity. Due to the correlated variability in the wave-3 ridges, the pronounced 16-year periods exist also in the surface temperature of southern Australia–New Zealand region, as well as in the zonal mean sea level pressure at 30°–50° S. The sea surface temperatures are much less involved in the 16-year oscillation suggesting that atmospheric rather than oceanic processes appear to be more important for its occurrence.

**Keywords** Antarctic Peninsula · Surface temperature · Austral winter · Periodicity

## 1 Introduction

The quasi-periodic variabilities of surface air temperature on the time scales from 2–8 years up to 20–80 years are well known from the global and regional climate studies based on time series of the climate indices (Park and Mann 2000; Parker et al. 2007). The interannual variations with the 2–8 year periods are mainly associated with the El-Niño–Southern Oscillation (ENSO) (Rasmusson and

Carpenter 1982; Neelin et al. 1998; Turner 2004). The decadal variability with the periods of 20–70 years is contributed by the Pacific Decadal Oscillation (PDO) and Interdecadal Pacific Oscillation (IPO) (Mantua et al. 1997; Parker et al. 2007; Meehl et al. 2009; Deser et al. 2010; Newman et al. 2016). The North Atlantic and European climate is known to be affected by the Atlantic Multidecadal Oscillation (AMO) on the time scale of 60–80 years (Schlesinger and Ramankutty 1994; Delworth and Mann 2000; Sutton and Hodson 2005). The intermitted interdecadal periods of 10–20 years are also present in the regional and global climate variability (Venegas et al. 1997; Park and Mann 2000; White and Tourre 2003; Mehta et al. 2018). Interference of the climate modes, their relative contributions to the temperature variability can evolve over decades and even cause climate regime shift, in particular in the Pacific Ocean basin (Trenberth et al. 2002; Meehl et al. 2009; Deser et al. 2010; Newman et al. 2016; Wang et al. 2019), and can influence (enhance or decelerate) the global temperature trends (Lin and Franzke 2015; Dai and Wang 2018).

✉ Oleksandr Evtushevsky  
o\_evtush@ukr.net

<sup>1</sup> Taras Shevchenko National University of Kyiv, Kyiv, Ukraine

<sup>2</sup> Space Sciences Laboratory, University of California Berkeley, Berkeley, CA, USA

<sup>3</sup> College of Physics, International Center of Future Science, Jilin University, Changchun, China

<sup>4</sup> Department of Atmosphere Physics and Geospace, National Antarctic Scientific Center, Kyiv, Ukraine

In the Southern Hemisphere (SH), it was shown that the Southern Annular Mode (SAM) (Marshall 2007; Fogt et al. 2012), Antarctic Circumpolar Wave (ACW) (Conolley 2003; Venegas 2003; White et al. 2004), and Antarctic Circumpolar Current (ACC) (Verdy et al. 2006) play a significant role on the interannual time scale (Carleton 2003). In the Antarctic Peninsula (AP) region, the ENSO–SAM–ACW–PDO coupling results in the varying relative influences of the individual climate mode on the temperature changes (Stastna 2010; Clem and Fogt 2013; Clem et al. 2016; Yu et al. 2015; Goodwin et al. 2016; Turner et al. 2020). The influence of the climate modes and their interactions depend on the season (Neelin et al. 1998; Marshall 2003; Yu et al. 2015), thereby affecting the seasonal change in the structure of quasi-stationary planetary waves (Hoskins and Karoly 1981; Wallace 1983; Yang and Webster 1990; Turner 2004; Raphael 2004; Fahad et al. 2021). The Rossby wave train forced by tropical Pacific heating anomalies (Karoly 1989; Mo and Higgins 1998; Fahad et al. 2021) reaches West Antarctica and the AP region, where quasi-stationary circulation anomalies are particularly strong during the austral winter (Turner 2004; Clem et al. 2016) and spring (Clem and Fogt 2013; Clem and Renwick 2015). Because of the variability in the ENSO–SAM coupling, regional circulation anomalies provide differences in the winter climate change in the different parts of the AP through redistribution of the zonal and meridional flows and dominant advection of warm or cold air towards the AP. A local decrease of sea level pressure can lead to greater cyclonic activity to the west, north or east of the AP in the Amundsen–Bellingshausen Seas, Drake Passage or Weddell Sea, respectively (Clem and Renwick 2015; Turner et al. 2016; Evtushevsky et al. 2020), influencing the temperature change across the AP. Owing to the multiplicity of interactions between the climate modes and to the relatively short records, the most important factors affecting the Antarctic temperatures are still unclear (Turner et al. 2020) and need to be determined.

The interdecadal variability of the AP winter surface temperature with the 16-year periodicity has been described in (Kravchenko et al. 2011) based on the Scientific Committee on Antarctic Research (SCAR) Reference Antarctic Data for Environmental Research (READER) from the early 1950s to 2009. Kravchenko et al. (2011) showed that the 3–8 year periods related to the ENSO, SAM and ACW signals were clearly separated from the 16-year oscillation. The most pronounced 16-year signals were observed in the time series from the northern AP stations. However, the source of the 16-year oscillation has not been identified in that work. Since this periodicity, according to (Kravchenko et al. 2011), appears only in the northern AP, presumably, it can be generated locally. In this paper we examine the localization of the prevalence of the 16-year periodicity in the AP region on

a longer time series and determine its possible source making use of the READER surface temperature data from the AP weather stations (Esperanza, Orcadas, and Vernadsky). The data description and analysis technique are presented in Sect. 2, and the results are presented in Sect. 3. The identification of the source of 16-year periodicity is described in Sect. 4. The results are discussed in Sect. 5, and the conclusions are presented in Sect. 6.

## 2 Data and analysis method

The time series of the surface air temperature recorded at Esperanza (ESP hereafter; the northern tip of the AP: 63.4° S, 57.0° W, 13 m; Fig. 1) is among the longest ones collected in the AP region. As was shown by Kravchenko et al. (2011), the ESP winter temperature in 1952–2009 reveals rather stable periodicity with the about 16-year cycle (their Fig. 3). We use the READER database (Turner et al. 2004) to process the AP station data sets: ESP (1952–2019, time series length is 68 years), Orcadas (ORC; 1903–2019, 117 years), and Faraday/Vernadsky (FV; 1951–2019, 69 years; the British station Faraday before and the Ukrainian station Vernadsky after 1996) from <https://legacy.bas.ac.uk/met/READER/data.html> (see the location of the stations in Fig. 1). ESP and ORC (FV) are in the northern (southern) AP region that determines their different sensitivity to the individual climate modes (King 1994; Vaughan et al. 2003; Turner et al. 2005; Oliva et al. 2017).

The linearly detrended and standardized data sets averaged over the austral winter months June, July and August (JJA) were analyzed making use of the Fast Fourier Transform (FFT) and the wavelet transform similar to



**Fig. 1** The region of the Antarctic Peninsula and the location of three weather stations Orcadas, Esperanza and Faraday/Vernadsky (closed circles) chosen for the analysis of the winter temperature periodicity

(Kravchenko et al. 2011). The FFT is useful to extract frequency (periodic) content of harmonics in a time series and wavelet analysis can determine both the dominant modes of variability and how those modes vary in time (Torrence and Compo 1998). Because the wavelet function is in general complex, the wavelet transform can be divided into the real and imaginary part (or amplitude and phase). Among the wavelet functions, the Morlet wavelet contains more oscillations and gives finer resolution (Torrence and Compo 1998), and it is used in this analysis. We analyze the time series of winter temperatures, since the Antarctic stations have generally their largest interannual variability of temperature during the winter and the annual mean temperature anomalies are dominated by winter temperatures (Turner et al. 2020).

To identify the possible source of the 16-year periodicity in the SH atmospheric variables, we have created an index of the local surface temperature variability. Considering the results of (Kravchenko et al. 2011), it is based on the ESP temperature anomalies (thin curve in Fig. 2a) with band pass filter in the period range of 15–17 years, or the frequency range of  $0.067\text{--}0.059\text{ year}^{-1}$  (thick curve in Fig. 2a). As the band pass filter is centered at the 16-year period and the filtered time series is of sine wave form (Fig. 2a), the latter is used as the sine wave index SW16 in this work. The peak at the 16-year period (or frequency  $0.0625\text{ year}^{-1}$ ) is clearly reproduced in the SW16 spectrum (marked with a vertical dashed line in Fig. 2b).

The SW16 index is used in the correlation analysis aimed at detecting the response of meteorological variables to the 16-year period signal. The data and analysis tools from the National Centers for Environmental Prediction (NCEP)–National Center for Atmospheric Research (NCAR) reanalysis (NNR; Kalnay et al. 1996; [www.esrl.noaa.gov/psd](http://www.esrl.noaa.gov/psd)) are used to determine the correlative relationships between SW16, sea level pressure (SLP), surface air

temperature (T-surface), surface zonal (U) and meridional (V) winds. Using the NNR monthly mean gridded variables averaged over June–August, the linear correlations for the Southern Hemisphere were processed (<https://psl.noaa.gov/data/correlation/>). The Marshall SAM index in the winter season was taken from <https://legacy.bas.ac.uk/met/gjma/sam.html> (Marshall 2003). An alternative index for the SH annular mode known as the Antarctic Oscillation (AAO; Gong and Wang 1999) was also used (<https://psl.noaa.gov/data/climateindices/>). Both indices characterize mass exchange between middle and high latitudes with perturbations in atmospheric parameters (e.g. zonal wind, geopotential height or sea level pressure) of opposite signs.

### 3 Frequency analysis

Figure 3 shows the time series (left) and FFT spectra (right) of the winter surface temperatures recorded at ESP (the top panel), ORC (the middle panel), and FV (the bottom panel). The decadal trends and their significance indicated in Fig. 3 (left) are consistent with the ones estimated from the shorter time series (King et al. 2003; Turner et al. 2005, 2020; Zazulie et al. 2010; Zitto et al. 2016).

The spectral power plots in Fig. 3 (right) show presence of the 2–7 year periods (2–9 years for FV) typical for the interannual variability in the climate modes ENSO, SAM, and ACW (see Sect. 1). The spectral peaks around 16, 16, and 18 years in the ESP, ORC, and FV data, respectively, have the amplitudes similar to the shorter period peaks. It was noted by Kravchenko et al. (2011) that the decadal periodicity in the AP climate variability is not inferior to the SH climate modes in climatic influences. This was confirmed by similar spectral power and statistical significance of the

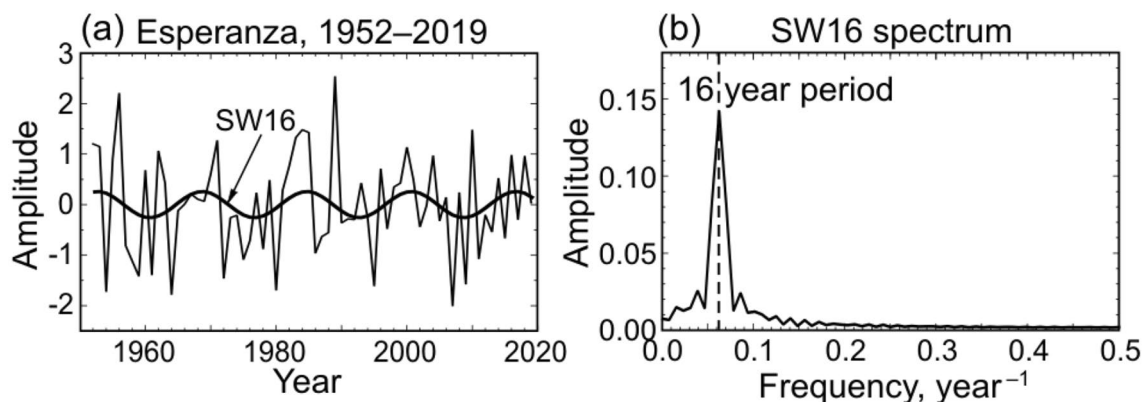
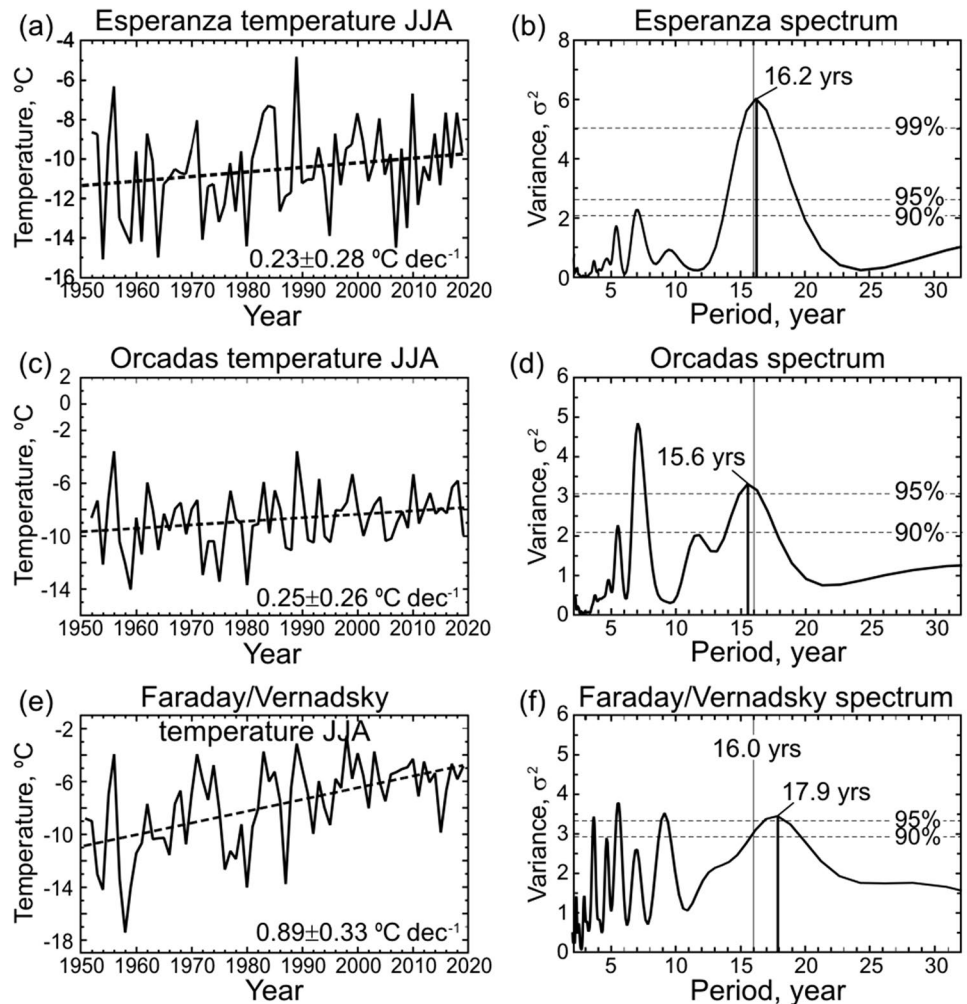


**Fig. 2** **a** Time series of surface temperature at Esperanza: detrended and standardized (thin curve), filtered with a band pass filter in the frequency range of  $0.067\text{--}0.059\text{ year}^{-1}$ , or the period range of

15–17 years (sine wave SW16 shown by thick curve). **b** The FFT spectrum of band-pass filtered time series

**Fig. 3** (Left) Time series of the winter surface temperature observed at **a** Esperanza, **c** Orcadas, and **e** Faraday/Vernadsky. The linear trends (dashed lines) with the 95% confidence intervals are presented at the bottom of the panels. (Right) The corresponding spectral power plots (**b**), (**d**), and (**f**) for time series (**a**), (**c**) and (**e**), respectively. The dashed lines indicate the 90%, 95%, and 99% confidence levels



temperature oscillations with the periods of three to eight years (associated with ENSO, SAM and ACW variability) and with the 16-year period (Kravchenko et al. 2011, their Figs. 4, 5, 6).

There is a difference between the stations in the presence of statistically significant periods on the interdecadal

time scale. In the ESP (ORC) spectrum in Fig. 3b (3d), there is a period of 16.2 years (15.6 years) with the 99% (95%) confidence level. This spectral peak is the strongest and most distinct one in the ESP time series. In the FV spectrum, the interdecadal peak is shifted to the longer period of 17.9 years (with the 95% significance). This peak

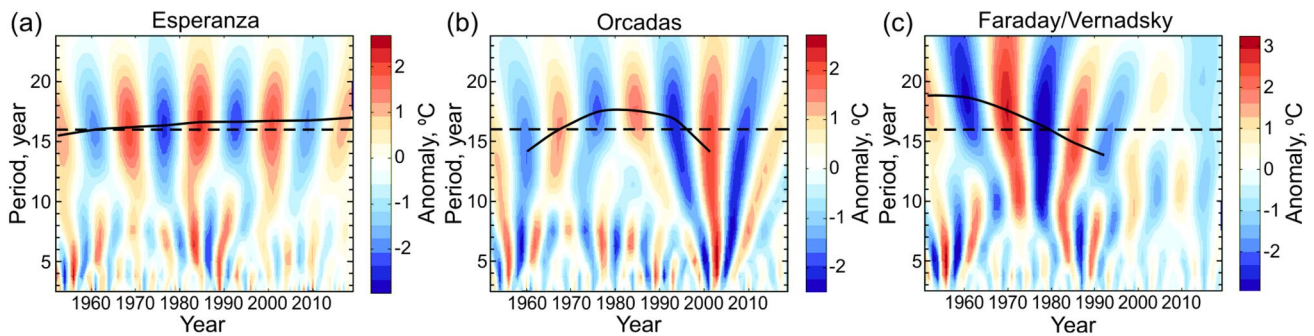
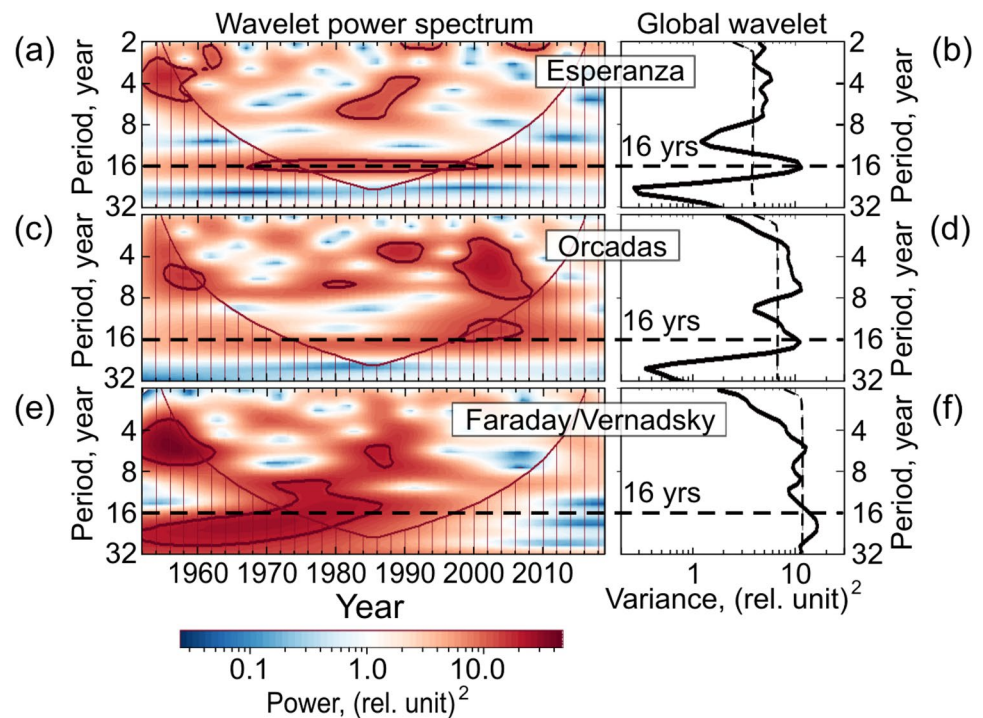


**Fig. 4** Wavelet spectra (the real component of the Morlet wavelet transform) of the austral winter temperature time series 1952–2019: **a** Esperanza, **b** Orcadas, and **c** Faraday/Vernadsky. The dashed line

indicates the 16-year period. The solid curves represent the change of the interdecadal periods



**Fig. 5** Wavelet power spectra (in the left) and the global wavelet spectra (in the right) of the winter temperature time series from **a, b** Esperanza, **c, d** Orcadas, and **e, f** Faraday/Vernadsky. The horizontal dashed line indicates the 16-year period. The contours in panels (**a, c, e**) and the vertical dashed lines in panels (**b, d, f**) indicate the 95% confidence level



is less distinct and broadens to a band of 16–20 years at the 90% confidence level (Fig. 3f) compared to the nearly 16-year peak in the ESP spectrum, which is narrower and higher (Fig. 3b).

The wavelet spectra in Fig. 4 (the real component) and Fig. 5 (the spectral power) emphasize the difference of the interdecadal period change in the time series recorded at the different stations. Figure 4 shows how periodic components vary in time and Fig. 5 gives global wavelet spectrum, which is obtained by integration of the wavelet power spectrum over time (Torrence and Compo 1998). The most persistent 16-year oscillation is in the winter temperature time series from ESP (Figs. 4a and 5a). The wavelet spectra peak slowly varies between 15 and 17 years (the solid curve in Fig. 4a) around the 16-year period (the dashed line in Fig. 4a) in 1952–2019. In addition to that in the FFT spectrum (Fig. 3b), there is a narrow spectral band in the wavelet power spectrum (Fig. 5a) and a strong peak in global wavelet spectrum (Fig. 5b), all statistically significant at the 95% confidence level.

The observed interdecadal periodicity is less stable in the ORC wavelet spectrum (1952–2019) and the peaks of the amplitude anomalies show variations of the period between 14 and 18 years (the solid curve in Fig. 4b). The greatest anomaly variations were in the 1980s–2000s (Fig. 4b), which makes the main contribution to statistically significant signals about 16-year in the Fourier spectrum (the 95% confidence level, Fig. 3d) and in the global wavelet spectrum (with the 95% confidence level, Fig. 5d).

No significant interdecadal periods were observed in the ORC time series between the 1900s and 1950s (Fig. S1a).

The least stable periodicity is seen from the FV wavelet transform. The observed period decreases from 19 to 14 years (Fig. 4c) and statistically significant signal in the wavelet power spectrum exists during 1950s–1980s (i.e., it characterizes only the first half of the time series, Fig. 5e). Compared to Esperanza, the interdecadal peak in the Faraday/Vernadsky spectrum is shifted to an 18-year period (Figs. 3f and 5f).

As noted from Fig. 3 (right) and seen in Fig. 4, the shorter periods (2–7 years) are observed in the ESP and ORC data than in the FV data (2–9 years). This difference between the FV and ESP–ORC time series is presumably related to the varying relative contributions of the individual climate modes to the temperature change in different parts of the AP. Due to the stronger tropical connection in the Pacific sector, the western AP (and FV) in winter and spring is more influenced by ENSO (Sect. 1). The influence is produced by a tropically-forced Rossby wave train directed to the south, so that the ENSO correlation in winter and spring is consistently strongest with the western AP temperature (Clem et al. 2016; Turner et al. 2020). This is confirmed by the climatological relationships between the Niño 4 index and surface temperature and zonal wind at the 850 hPa pressure level for winter and spring (Fig. S4a–S4d). Unlike this, the temperatures at ESP and ORC located in the northern AP region are more

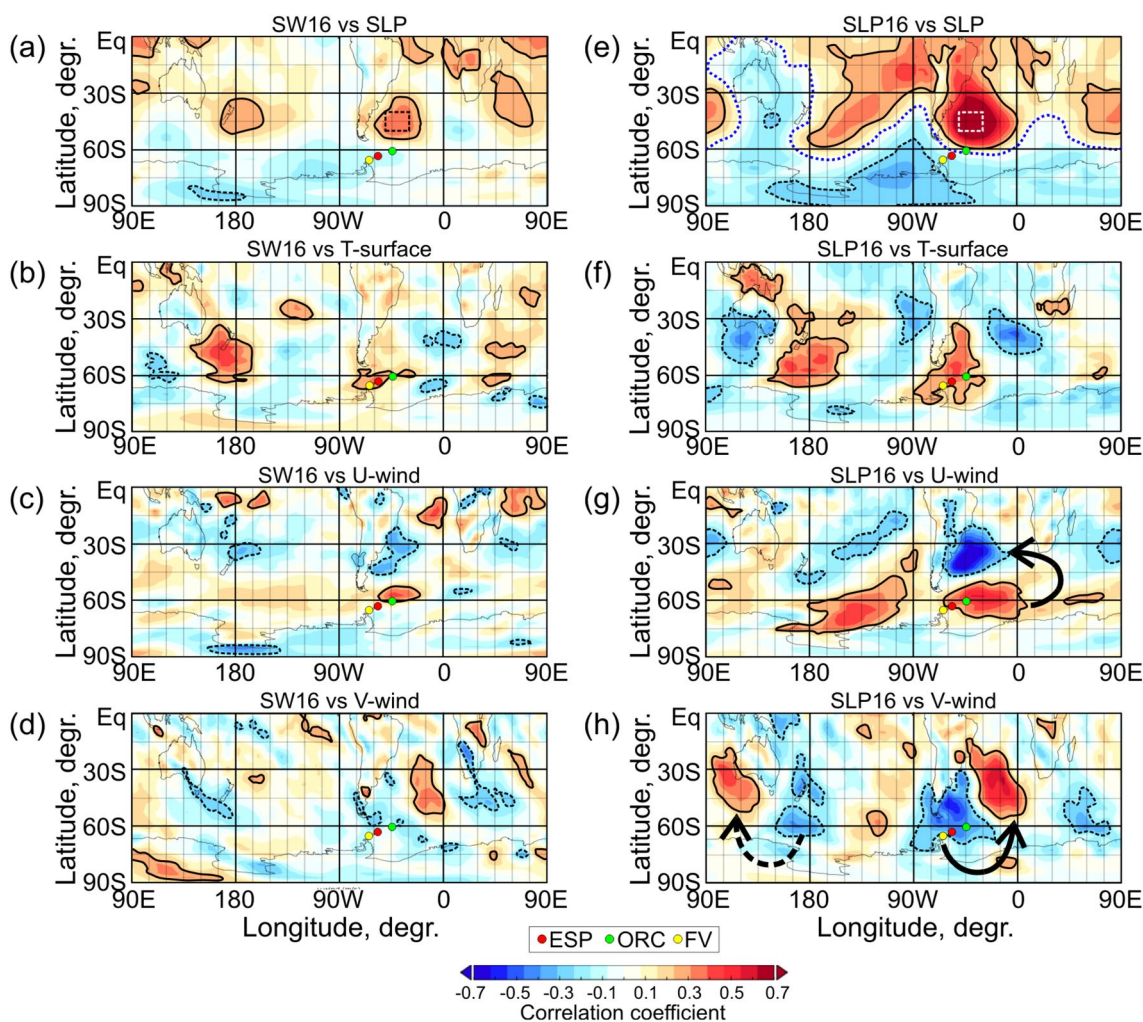


**Fig. 6** Correlation maps of the SW16 index with **a** the sea-level pressure SLP and **b** surface air temperature T, **c** the zonal wind U and **d** meridional wind V. Panels **(e, f, g and h)** present distributions of correlation of the SLP16 index with SLP, T, U, and V (see text for explanation). The solid (dashed) contours indicate the 95% signifi-

cance of positive (negative) correlation on the 68-year time series (1952–2019). The dashed rectangle in **(a)** and **(e)** outlines the SLP16 area. The colored circles indicate the location of the stations according to the legend below

influenced by zonal circulation and annular mode (Fig. S4e–S4h; see Sect. 5 for discussion).

#### 4 The source of the 16-year periodicity

The length of the analyzed time series is 68 years (Fig. 3, left) covering more than 4 full 16-year periods determined in the ESP temperature (Fig. 4a). An unusually stable oscillation is statistically significant (Figs. 2b and 5a, b) and requires the existence of equally long-acting sources.

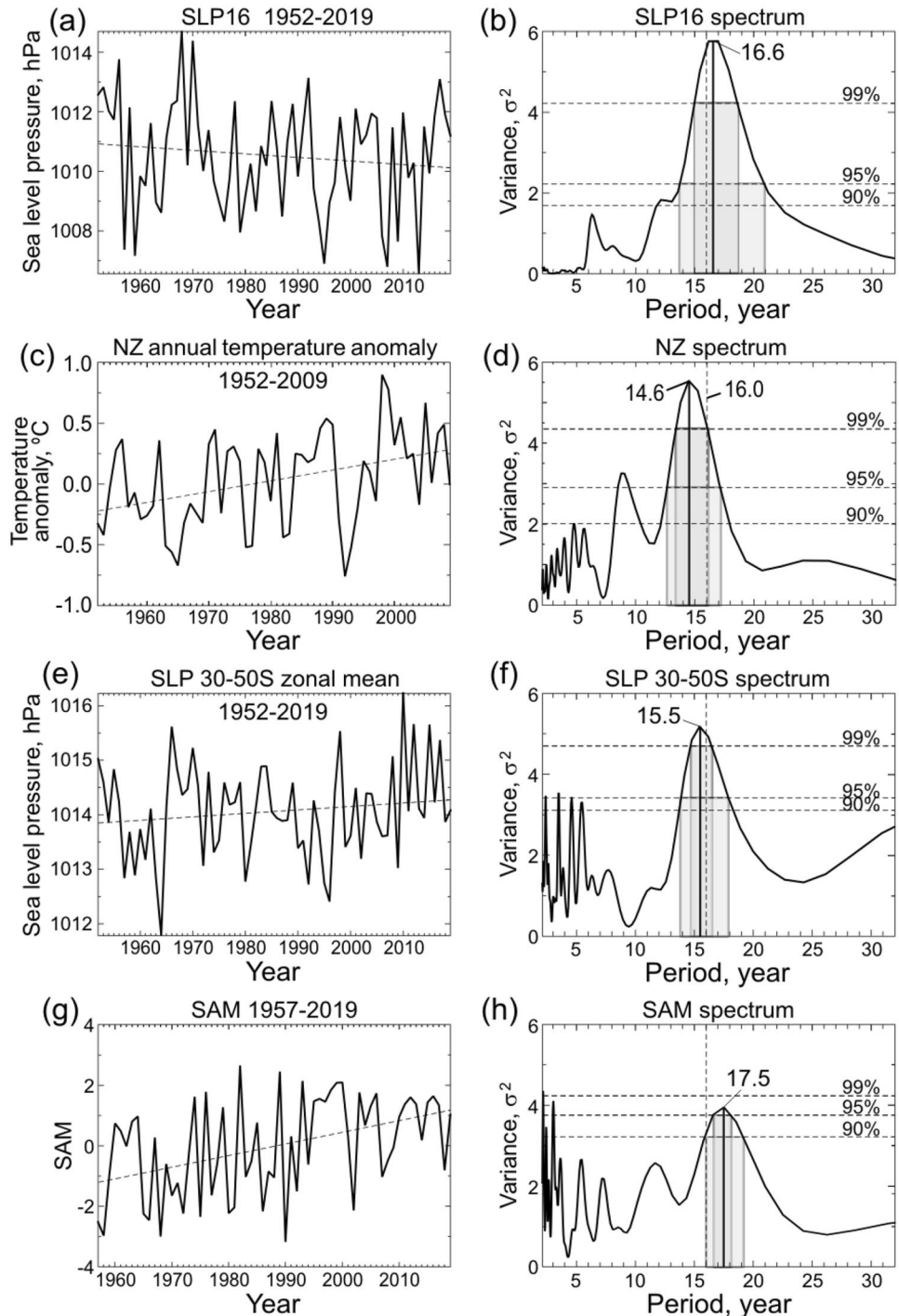
As described in Sect. 2, the SW16 index was introduced to quantitatively represent the 16-year periodicity in the ESP time series (Fig. 2). Based on the SW16 index, one can verify whether a source of this periodicity exists in the SH atmosphere variability.

Figure 6a–d displays anomalies in the spatial distribution of linear correlation coefficient  $r$  between SW16 and several SH atmospheric variables: sea level pressure SLP and surface air temperature and wind components. It is seen that the largest area of significant correlation anomalies is in the SLP response (Fig. 6a). Correlation anomalies in the SH subtropical and middle latitudes demonstrate zonal wave-3 pattern, represented by three positive correlation anomalies (Fig. 6a) alternating with negative ones (most pronounced in correlation with surface temperature in Fig. 6b). This quasi-stationary pattern in the SH atmosphere is determined by the alternation of three continents and three ocean basins (Raphael 2004) and three subtropical anticyclones (van Loon and Jenne 1972; Carleton 2003; al Fahad et al. 2020) in the longitudinal direction.

Less pronounced wave 3 patterns are observed in the correlations with the wind components (Fig. 6c, d). Correlation anomalies significant at the 95% confidence level exist over and in the vicinity of the AP region (Fig. 6b–d). The intense positive anomalies ( $r=0.3-0.6$ ) related to zonal wave 3 are seen in the New Zealand (NZ) region (Fig. 6a, b). They indicate a 16-year periodicity in the sea level pressure and surface temperature over a fairly large area. Indeed, even the

annual mean temperature observed in New Zealand (Fig. 7c) shows that the spectral band of 13.3–16.0 (12.7–17.2) years is statistically significant at the 99% (95%) confidence level (Fig. 7d). The peak in the wavelet power spectrum is at 14.6 years. This result is based on the NZ temperature records in 1952–2009 averaged over 11 stations (Fig. 7c) and available at the National Institute of Water and Atmospheric

**Fig. 7** (Left) The time series and (right) Fourier spectra of the variability indices: **a, b** the atmospheric pressure in the southwestern Atlantic, SLP16 (dashed rectangle in Fig. 6a); **c, d** the annual mean temperature anomaly in New Zealand averaged over 11 stations; **e, f** zonal mean SLP in 30°–50° S (index SLP30–50S), and **g, h** SAM. The solid (dashed) vertical line marks the period at the peak of the spectral power (16-year period). The spectral bands in the right column, significant at the 90%, 95% and 99% confidence levels, are shaded





Research (NIWA) web site <https://niwa.co.nz/climate/information-and-resources/nz-temperature-record>.

The SW16 index is coupled with the SLP anomalies of the anticyclone type: an increase in SW16 corresponds to an increase in the regional SLP anomaly. A strong positive anomaly in correlation ‘SW16 vs SLP’ located in the southwestern Atlantic (SWA, Fig. 6a) adjacent to the AP region indicates the close relationship between the anomalies in the SWA SLP and the ESP temperature on the interdecadal time scale.

The area of the maximal SLP response to SW16 limited by the coordinates of 40°–50° S, 30°–50° W (the dashed rectangle in Fig. 6a) was used to verify the correlations. The time series of area-averaged SLP anomalies inside this domain (Fig. 7a) was considered as the regional 16-year SLP variability index, SLP16. It is seen from Fig. 7b that the 16.6-year period clearly stands out in the spectrum of SLP16 (the solid vertical line) and spectral band of about 15–19 years is significant at the 99% confidence level (the shaded rectangle).

As noted above, the wave 3 ridges in Fig. 6a are located mainly in the SH subtropics and middle latitudes and their phase correlation with SW16 suggests the presence of close to 16-year period throughout this zone. The zonal mean SLP anomalies for 30°–50° S (characterized by the index SLP30–50S, Fig. 7e), demonstrate a close period of 15.5 years statistically significant at the 99% confidence level (Fig. 7f). The existence of this variability in the mid-latitude zone shows the important role of a periodicity close to 16 years as one of the most powerful modes in the SH climate change. Moreover, the correlation anomalies in Fig. 6 highlight certain areas where changes in SLP, surface temperature and wind components can affect the climate on an interdecadal time scale.

The coupling of the SLP16 index with the SH sea level pressure is shown in Fig. 6e. Correlation anomalies display zonal wave 3 (the blue dotted curve at zero correlation) and SAM (opposite anomalies in middle and high SH latitudes) patterns. It should be pointed out that the correlation coefficient distribution for both SW16 (Fig. 6a) and SLP16 (Fig. 6e) does not reveal statistically significant anomalies along the equatorial Pacific, characteristic of the El Niño phenomenon. Positive anomaly in correlation ‘SLP16 vs T-surface’ in the western tropical Pacific is evident (Fig. 6f), however, this is not a typical El Niño region located usually in the central and eastern Pacific (Rasmusson and Carpenter 1982; Trenberth et al. 2002). In addition, SW16 and SLP16 are weakly coupled not only with tropical surface air temperature (Fig. 6b, f), but also with the tropical sea surface temperature (SST; Fig. S2). Moreover, in the case of SST, no clear anomalies that resemble SAM or wave 3 patterns are evident (Fig. S2). Such relatively weak presence of the 16-year periodicity in the SST variability can indicate that

this spectral component is more associated with atmospheric than with oceanic processes.

We note that the SLP16 index correlates with T, U-wind and V-wind much stronger ( $r_{\max} = 0.6$ ; Fig. 6f–h) than the SW16 index ( $r_{\max} = 0.4$ ; Fig. 6b–d, respectively). Statistically significant correlation anomalies cover the northern part of AP, but do not reach its southern part. For U-wind and V-wind (Fig. 6g, h, respectively), they are statistically significant at ESP and ORC and not significant at FV (the stations’ locations are marked with the red, green and yellow circles respectively). The SLP16 effect in the surface temperature has a similar difference in significance but FV is located at the edge of the area outlined by the 95% significance contour (Fig. 6f). The influence of the SLP16 anomaly (Fig. 6a) on the AP region is, therefore, spatially limited and Fig. 6f–h clarifies why the 16-year oscillation can be more reliably recorded in the northern AP but not in the southern AP.

The relative position of positive and negative anomalies in the response of wind components to SLP16 exactly corresponds to anticyclonic (counterclockwise) circulation in South Atlantic and Weddell Sea (solid curved arrows in Fig. 6g, h). The positive correlation anomaly in the U-wind (V-wind) at the southern (eastern) edge of the SLP16 region in Fig. 6g (Fig. 6h) can be interpreted as a westerly (southerly) enhancement in response to the SLP16 index increase. This pattern is consistent with the structure of the anticyclonic wind (solid curved arrows in Fig. 6g, h) in the SH atmospheric circulation. In turn, the westerly enhancement (Fig. 6g) means greater transport of warm oceanic air to the northern AP. The latter has a 16-year component of variability due to periodic enhancement and weakening of the anticyclonic anomaly in the SLP16 region (Fig. 6a). A similar warming effect can be expected from the negative correlation anomaly in V-wind in the AP region (Fig. 6h) due to the cold southerly anomaly decrease (or, in terms of anticyclonic circulation, the warm northerly anomaly increase). Spatially, as noted above, ESP and ORC appear to be more sensitive to the 16-year periodicity (Fig. 6e–h) originating in the SLP16 region (Fig. 6a).

There is also a large-scale response to SLP16 containing the wave-3 and SAM patterns (Fig. 6e–h). Spectral properties of the wave-3 pattern are presented for the three regions: (i) the SWA region (peak at 16.6 years from the winter SLP16 index in Fig. 7b), (ii) the northern AP (16.2 and 15.6 years in the ESP and ORC winter temperature in Fig. 3b, d, respectively) and (iii) New Zealand (14.6 years in the annual mean temperature in Fig. 7d). Spectrum of winter SAM index shows a peak of spectral power at the 17.5-year period (Fig. 7h). Additionally, large-scale variability with strong period 15.5 years exists in 30°–50° S zonal mean SLP (Fig. 7f). Figure S3 shows that the zonal wave-3 and SAM patterns are even more evident in correlations with



the index SLP30–50S than in correlations with the index SLP16 (Fig. 6f–h).

In general, at least 5 indices of variability (SW16, SLP16, SLP30–50S, SAM, and NZ) demonstrate a noticeable prevalence of oscillation close to the 16-year period associated with quasi-stationary regional anomalies in the SH circulation. Surface temperature, SLP, and wind components in these anomalies undergo periodic changes on the interdecadal time scale (Fig. 6) and contribute to regional climate changes, which become both cyclical and synchronized. The effects of the 16-year periodicity in the regional couplings are the subject to study in a separate work. The main coupled regions are located at the wave 3 ridges in the SLP anomalies, which strongly correlate with the SW16 and SLP16 indices (Fig. 6a, e) and are associated with the zonal mean SLP variability (SLP30–50S index, Fig. 7f) and the annular mode pattern (SAM index, Fig. 7h).

A multiple linear regression model was analyzed using Esperanza's temperature as the dependent variable and the four indices (SW16, SLP16, SLP30–50S and NZ) treated as independent variables (Fig. S6). From the regression model, the square of the correlation coefficient  $R^2=0.33$  is significant at the 95% confidence level. This means that the near 16-year interdecadal periodicity provides a 33% contribution to the ESP temperature variability giving notable change in long-term trend.

We note that the east–west polarity of the correlation anomalies in the region of the southern Australia and New Zealand is opposite to the polarity in the southwestern Atlantic–Antarctic Peninsula region (Fig. 6f). This pattern suggests a cyclonic regional anomaly (dashed curved arrow in Fig. 6h). According to the generalized results, the periodicities between about 13 and 21 years centered close to 16-year period are statistically significant at the 95% confidence level (Fig. 3b; shaded rectangles in Fig. 7, right).

We also examined the spectral features of surface temperature variations in the AP region (Fig. S5) using the NCEP–NCAR reanalysis data. Four domains were chosen in: northeastern (N–E) AP, southwestern (S–W) AP, Orcadas area (latitude  $\times$  longitude =  $5^\circ \times 10^\circ$ ) and South Pacific region ( $10^\circ \times 10^\circ$ ), as shown by the shaded rectangles in Fig. S5e. The degree of consistency of interdecadal spectral peaks with station data was determined. The spectra were compared in pairs: N–E AP vs ESP, Orcadas area vs ORC, and S–W AP vs FV. Table 1 shows that the reanalysis reliably reproduces even small spatial differences in spectral peaks observed from the station data. In South Pacific domain further west of the peninsula, there is no periodicity close to 16 years (Table 1 and Fig. S5a).

Finally, the wavelet spectra show that the interdecadal temperature oscillation in 2000s to 2010s exhibits transition

**Table 1** Comparison of interdecadal periods in the spectra of surface temperature time series from the station data in the AP region (Esperanza, Orcadas and Faraday/Vernadsky) and from the NCEP–NCAR reanalysis (NNR) for the three sub-regions (N–E AP, Orcadas area and S–W AP, respectively), and additionally for the South Pacific sub-region

Station	Esperanza	Orcadas	Faraday/Vernadsky	
(Fig. 3)	16.2	15.6	17.9	
NNR	N–E AP	Orcadas area	S–W AP	South Pacific
(Fig. S5)	16.1	15.2	17.9	11.5, 21.3

The spectra are compared in Fig. S5a–S5d, and the boundaries of the sub-regions are shown in Fig. S5e

from the negative to positive phases at Esperanza and Orcadas (Fig. 4a, b) and from positive to negative phases at Faraday/Vernadsky (Fig. 4c). This result is consistent with the trends in the temperature time series observed recently: warming (Fig. 3a, c) and cooling (or no warming, Fig. 3e), respectively (Oliva et al. 2017; Evtushevsky et al. 2020).

## 5 Discussion

In the Antarctic temperature, the 10–20-year periods are likely to be of PDO signal (Rahaman et al. 2019). PDO is determined by the SST anomalies, i.e. it characterizes the state of ocean. By our estimate for the winter 1952–2017 time series, PDO shows strong peaks only in 9–12 and 40–60 year period ranges (not shown) that excludes notable effects in the interdecadal range. The oceanic circulation anomalies in the SWA region known as the Brazil–Malvinas Confluence (da Silveira and Pezzi 2014) and the Zapiola Anticyclone (Venaille et al. 2011) are varying mainly on an interannual time scale.

In the atmospheric parameters, the SLP fluctuations in the South Atlantic dominate in the interdecadal timescale at a 14–16-yr period caused by oscillation in the strength of the subtropical anticyclone (SA) with its center at around  $30^\circ$  S (Venegas et al. 1997). An action area of SA is  $15^\circ$ – $45^\circ$  S and  $45^\circ$  W– $15^\circ$  E (Mächel et al. 1998). Climatologically, SA is located to east of the SLP16 anomaly and closer to the West Africa coast. However, it extends to the east coast of South America (to about  $45^\circ$ – $50^\circ$  W) in the austral winter (Reboita et al. 2019), overlapping partly the SLP16 region ( $40^\circ$ – $50^\circ$  S,  $30^\circ$ – $50^\circ$  W, rectangle in Fig. 6a, e). This pattern suggests a potential contribution of SA to a 16-year periodicity. It should be especially noted that SA is part of the zone  $30^\circ$ – $50^\circ$  S, which is characterized by a strong spectral peak at a 16-year period (Fig. 7f). There are the influences of the tropics on the southern subtropical anticyclones, which depend on the season. They are realized through variability in ENSO

(Venegas et al. 1997), the summer monsoons and heating in the tropical Northern Hemisphere (Yang and Webster 1990; Lee et al. 2013), Intertropical Convergence Zone (Mächel et al. 1998) or South Pacific Convergence zone (Clem and Renwick 2015; Fahad et al. 2021). However, our results indicate that in winter there is a dominant extratropical contribution to the 16-year periodicity under consideration (Fig. 6 and Fig. S2).

As noted in Sect. 3, the difference between the SH circulation anomalies forced in the tropics and in the extratropics is illustrated in Fig. S4. Correlations between climate modes Niño 4 (N4) and Antarctic Oscillation [AAO, an index alternative to SAM, e.g. (Gong and Wang 1999)], on the one hand, and the surface temperature and zonal wind in the lower troposphere (850 hPa), on the other hand, are compared. In the first case, the central tropical Pacific mode N4 in winter and spring is associated with the planetary wave train propagated within the Pacific basin toward West Antarctic (thick dashed line in Fig. S4c and S4d). The negative temperature response is concentrated mainly in the western AP (white contour in Fig. S4a and S4b). In the second case, the annular mode exhibits response in zonally-oriented anomaly sequence at mid and high latitudes (dashed curves in Fig. S4g and S4h) without any anomalies in the tropics. The positive temperature response is clearly seen in the northern AP region (black contour in Fig. S4e and S4f).

As shown by Marshall (2007), a boundary between the regions where temperatures are positively and negatively correlated with SAM exists, and the line that separates these regions moves through the FV latitude twice a year. The recent SAM-related winter deepening of the negative SLP anomaly to the west of the AP, accompanied by a change in the zonal and meridional wind components, also contributes to the occurrence of the boundary that crosses the AP and divides it into sub-regions with warming and cooling (Evtushevsky et al. 2020). In the interannual temperature variations, the difference between SAM (prevailing periods of 2–5 years) and ENSO (2–8 years) (Yuan and Yonekura 2011; Rahaman et al. 2019) seems to correspond to the difference between ESP–ORC and FV, respectively, in their spectra (Fig. 3, right, and Fig. 4).

It is quite expected that the distribution of statistically significant anomalies in the correlation between the SLP30–50S index and the surface zonal wind demonstrates a zonal arrangement (Fig. S3b), very similar to the climatological SAM pattern (Fig. S4c). This is because the 30°–50° S latitude band corresponds to the midlatitude part of annular mode variability (Gong and Wang 1999; Marshall 2003). In the SH midlatitudes, SAM in winter exhibits a pronounced zonal asymmetry with the structure of wave 3 (Gong and Wang 1999; Fogt et al. 2012; Yeo and Kim 2015; Spensberger et al. 2020) seen also from climatological relationships in Figs. S3b, S3c, S4g and S4h.

Likewise, the correlations of annual mean temperature from the AP stations with annual mean SLP for 1979–2014 show clear wave-3 pattern combined with the SAM pattern (Turner et al. 2016; their Extended Data Fig. 6). In (Turner et al. 2016), the strongest correlation anomaly (up to  $r=0.8$ ) in the SWA region appears only for the northern AP stations (Bellingshausen, O’Higgins, Esperanza and Marambio), consistent with Fig. 6a above.

There is uncertainty in the detection of periodic oscillations caused by the difference in the indices of variability used in this analysis, because they show dependence of the spectral composition on the region, season, and also on the time range of the dataset and its length (Torrence and Compo 1998; Park and Mann 2000; Lin and Franzke 2015; Godoi et al. 2016). In our analysis, the region (northern AP), the season (austral winter) and the observed 16-year periods are known, and we are looking for other regions that serve as a source of or involved in the 16-year periodicity. This approach allows us to study in more detail the factors associated with the appearance of this periodicity, thereby partially answering some questions that remain regarding how modes of variability in various parts of the world influence Antarctic temperatures (Turner et al. 2020).

As noted in Sect. 1, natural decadal oscillations can enhance or decelerate long-term temperature trends (Lin and Franzke 2015; Dai and Wang 2018). Evidence of this effect was noted in Sect. 3 when comparing Fig. 4 and Fig. 3 (left). If interdecadal oscillations (10–20 year period range) in the 2000s and 2010s shift the phase from negative to positive on ESP and ORC (Fig. 4a, b), then the opposite phase shift is observed on FV (Fig. 4c). This is consistent with positive and negative (or near-zero) temperature trends in the respective parts of the time series (Fig. 3a, c vs Fig. 3e). A similar difference in recent climate change along the peninsula was noted in (Turner et al. 2016, 2020; Oliva et al. 2017; Evtushevsky et al. 2020).

## 6 Conclusions

In this work we confirm the persistent 16-year periodicity in the winter temperature [found in earlier study by Kravchenko et al. (2011)] at the northern Antarctic Peninsula station Esperanza on the longer time series, and determine the source of this periodicity by studying how widespread it is in the Southern Hemisphere, additional to the AP region.

Correlation analysis with the sea level pressure revealed regions of the strongest response to the 16 years period. The correlation anomalies, which are statistically significant at the 95% confidence level, fall on the SH subtropics and mid-latitudes (30°–50° S, Fig. 6a). Three areas of positive SLP response to the 16-year temperature periodicity resemble the zonal wave-3 pattern in the distribution of subtropical

anticyclones. The strongest correlation anomaly is located in the southwestern Atlantic. It partially overlaps with the subtropical anticyclone in the South Atlantic and, at the same time, is adjacent to the AP region.

This regional anomaly is associated with variations in the zonal and meridional wind components that affect the temperature in the southwestern Atlantic and the AP region. The correlation maps show that this influence is more significant in the northern AP. Therefore, the 16-year period is more clearly manifested in the winter temperature spectra from Esperanza and Orcadas in the northern AP region than at Faraday/Vernadsky in the southern AP region.

The 16-year periodicity is found in the regional temperature variability index, zonal mean sea level pressure in 30°–50° S, Southern Annular Mode index, and New Zealand temperature periodograms. However, the regional SLP index has a negligible correlation with sea surface temperature in the tropical Pacific, which excludes the El Niño phenomenon as a factor influencing the origin and evolution of the 16-year periodicity. This result indicates that the atmospheric rather than oceanic processes are more important for the stability of this oscillation. Our results highlight the two regions with the pronounced 16-year periods in the surface temperature dynamics: the southwest Atlantic–Antarctic Peninsula and southern Australia–New Zealand. The interdecadal variability in our results contributes to changes in temperature trends, modulates regional warming and cooling in the Southern Hemisphere and, thus, should be taken into account when creating and improving climate models.

**Supplementary Information** The online version contains supplementary material available at <https://doi.org/10.1007/s00382-021-05886-7>.

**Acknowledgements** We acknowledge the SCAR READER database for free access to the monthly data of the Antarctic station surface meteorology, available at <https://legacy.bas.ac.uk/met/READER/>. NCEP–NCAR Reanalysis data and images were provided by the NOAA/OAR/ESRL PSD, Boulder, Colorado, USA, from their Web site at <http://www.esrl.noaa.gov/psd/>. This work was partly supported by Taras Shevchenko National University of Kyiv, Ukraine, project 19BF051-08.

**Data availability** The data used in this study was downloaded from open sources (e.g. <https://legacy.bas.ac.uk/met/READER/>, <http://www.esrl.noaa.gov/psd/>).

## Declarations

**Conflict of interest** The authors have no conflicts of interests to declare that are relevant to the content of this article.

## References

- al Fahad A, Burls NJ, Strasberg Z (2020) How will southern hemisphere subtropical anticyclones respond to global warming? Mechanisms and seasonality in CMIP5 and CMIP6 model projections. *Clim Dyn* 55:703–718. <https://doi.org/10.1007/s00382-020-05290-7>
- Carleton AM (2003) Atmospheric teleconnections involving the Southern Ocean. *J Geophys Res* 108:8080. <https://doi.org/10.1029/2000JC000379>
- Clem KR, Fogt RL (2013) Varying roles of ENSO and SAM on the Antarctic Peninsula climate in austral spring. *J Geophys Res Atmos* 118:11481–11492. <https://doi.org/10.1002/jgrd.50860>
- Clem KR, Renwick JA (2015) Austral spring Southern Hemisphere circulation and temperature changes and links to the SPCZ. *J Clim* 28:7371–7384. <https://doi.org/10.1175/JCLI-D-15-0125.1>
- Clem KR, Renwick JA, McGregor J, Fogt RL (2016) The relative influence of ENSO and SAM on Antarctic Peninsula climate. *J Geophys Res Atmos* 121:9324–9341. <https://doi.org/10.1002/2016JD025305>
- Connolley WM (2003) Long-term variation of the Antarctic Circumpolar Wave. *J Geophys Res* 108:8076. <https://doi.org/10.1029/2000JC000380>
- da Silveira IP, Pezzi LP (2014) Sea surface temperature anomalies driven by oceanic local forcing in the Brazil–Malvinas Confluence. *Ocean Dyn* 64:347–360. <https://doi.org/10.1007/s10236-014-0699-4>
- Dai X, Wang P (2018) Identifying the early 2000s hiatus associated with internal climate variability. *Sci Rep* 8:13602. <https://doi.org/10.1038/s41598-018-31862-z>
- Delworth T, Mann M (2000) Observed and simulated multidecadal variability in the Northern Hemisphere. *Clim Dyn* 16:661–676. <https://doi.org/10.1007/s003820000075>
- Deser C, Alexander MA, Xie SP, Phillips AS (2010) Sea surface temperature variability: patterns and mechanisms. *Ann Rev Mar Sci* 2:115–143. <https://doi.org/10.1146/annurev-marine-120408-151453>
- Evtushevsky OM, Kravchenko VO, Grytsai AV, Milinevsky GP (2020) Winter climate change on the northern and southern Antarctic Peninsula. *Antarct Sci* 32:408–424. <https://doi.org/10.1017/S0954102020000255>
- Fahad AA, Burls NJ, Swenson ET, Straus DM (2021) The influence of South Pacific Convergence Zone heating on the South Pacific subtropical anticyclone. *J Clim* 34:3787–3798. <https://doi.org/10.1175/JCLI-D-20-0509.1>
- Fogt RL, Jones JM, Renwick J (2012) Seasonal zonal asymmetries in the Southern Annular Mode and their impact on regional temperature anomalies. *J Clim* 25:6253–6270. <https://doi.org/10.1175/JCLI-D-11-00474.1>
- Godoi VA, Bryan KR, Gorman RM (2016) Regional influence of climate patterns on the wave climate of the southwestern Pacific: the New Zealand region. *J Geophys Res Oceans* 121:4056–4076. <https://doi.org/10.1002/2015JC011572>
- Gong D, Wang S (1999) Definition of Antarctic Oscillation index. *Geophys Res Lett* 26:459–462. <https://doi.org/10.1029/1999GL900003>
- Goodwin BP, Mosley-Thompson E, Wilson AB, Porter SE, Sierra-Hernandez MR (2016) Accumulation variability in the Antarctic Peninsula: the role of large-scale atmospheric oscillations and their interactions. *J Clim* 29:2579–2596. <https://doi.org/10.1175/JCLI-D-15-0354.1>
- Hoskins BJ, Karoly DJ (1981) The steady linear response of a spherical atmosphere to thermal and orographic forcing. *J Atmos Sci* 38:1179–1196. [https://doi.org/10.1175/1520-0469\(1981\)038%3c1179:TSLROA%3e2.0.CO;2](https://doi.org/10.1175/1520-0469(1981)038%3c1179:TSLROA%3e2.0.CO;2)



- Kalnay E, Kanamitsu M, Kistler R, Collins W, Deaven D, Gandin L, Iredell M, Saha S, White G, Woollen J, Zhu Y, Chelliah M, Ebisuzaki W, Higgins W, Janowiak J, Mo KC, Ropelewski C, Wang J, Leetmaa A, Reynolds R, Jenne R, Joseph D (1996) The NCEP–NCAR 40-year reanalysis project. *Bull Am Meteorol Soc* 77:1057–1072. [https://doi.org/10.1175/1520-0477\(1996\)077%3C0437:TNYRP%3E2.0.CO;2](https://doi.org/10.1175/1520-0477(1996)077%3C0437:TNYRP%3E2.0.CO;2)
- Karoly DJ (1989) Southern Hemisphere circulation features associated with El Niño–Southern Oscillation events. *J Clim* 2:1239–1252. [https://doi.org/10.1175/1520-0442\(1989\)002%3c1239:SHC-FAW%3e2.0.CO;2](https://doi.org/10.1175/1520-0442(1989)002%3c1239:SHC-FAW%3e2.0.CO;2)
- King JC (1994) Recent climate variability in the vicinity of the Antarctic Peninsula. *Int J Climatol* 14:357–369. <https://doi.org/10.1002/joc.3370140402>
- King JC, Turner J, Marshall GJ, Connolley WM, Lachlan-Cope TA (2003) Antarctic Peninsula climate variability and its causes as revealed by analysis of instrumental records. *Antarct Res Ser* 79:17–30. <https://doi.org/10.1029/AR079p0017>
- Kravchenko VO, Evtushevsky OM, Grytsai AV, Milinevsky GP (2011) Decadal variability of winter temperatures in the Antarctic Peninsula region. *Antarct Sci* 23:614–622. <https://doi.org/10.1017/S0954102011000423>
- Lee SK, Mechoso CR, Wang C, Neelin JD (2013) Interhemispheric influence of the northern summer monsoons on southern subtropical anticyclones. *J Clim* 26:10193–10204. <https://doi.org/10.1175/JCLI-D-13-00106.1>
- Lin Y, Franzke CLE (2015) Scale-dependency of the global mean surface temperature trend and its implication for the recent hiatus of global warming. *Sci Rep* 5:12971. <https://doi.org/10.1038/srep12971>
- Mächel H, Kapala A, Flohn H (1998) Behaviour of the centres of action above the Atlantic since 1881. Part I: characteristics of seasonal and interannual variability. *Int J Climatol* 18:1–22. [https://doi.org/10.1002/\(SICI\)1097-0088\(199801\)18:1%3c1::AID-JOC225%3e3.0.CO;2-A](https://doi.org/10.1002/(SICI)1097-0088(199801)18:1%3c1::AID-JOC225%3e3.0.CO;2-A)
- Mantua NJ, Hare SR, Zhang Y, Wallace JM, Francis RC (1997) A Pacific interdecadal climate oscillation with impacts on salmon production. *Bull Am Meteorol Soc* 78:1069–1080. [https://doi.org/10.1175/1520-0477\(1997\)078%3c1069:APICOW%3e2.0.CO;2](https://doi.org/10.1175/1520-0477(1997)078%3c1069:APICOW%3e2.0.CO;2)
- Marshall GJ (2003) Trends in the Southern Annular Mode from observations and reanalyses. *J Clim* 16:4134–4143. <https://doi.org/10.1175/1520-0442%282003%29016%3c4134%3ATITSAM%3e2.0.CO;3B2>
- Marshall GJ (2007) Half-century seasonal relationships between the Southern Annular Mode and Antarctic temperatures. *Int J Climatol* 27:373–383. <https://doi.org/10.1002/joc.1407>
- Meehl GA, Hu A, Santer BD (2009) The mid-1970s climate shift in the Pacific and the relative roles of forced versus inherent decadal variability. *J Clim* 22:780–792. <https://doi.org/10.1175/2008JCLI2552.1>
- Mehta VM, Wang H, Mendoza K (2018) Simulations of three natural decadal climate variability phenomena in CMIP5 experiments with the UKMO HadCM3, GFDL-CM2.1, NCAR-CCSM4, and MIROC5 global earth system models. *Clim Dyn* 51:1559–1584. <https://doi.org/10.1007/s00382-017-3971-8>
- Mo KC, Higgins RW (1998) The Pacific–South American modes and tropical convection during the Southern Hemisphere winter. *Mon Weather Rev* 126:1581–1596. [https://doi.org/10.1175/1520-0493\(1998\)126%3c1581:TPSAMA%3e2.0.CO;2](https://doi.org/10.1175/1520-0493(1998)126%3c1581:TPSAMA%3e2.0.CO;2)
- Neelin JD, Battisti DS, Hirst AC, Jin FF, Wakata Y, Yamagata T, Zebiak SE (1998) ENSO theory. *J Geophys Res* 103:14261–14290. <https://doi.org/10.1029/97JC03424>
- Newman M, Alexander MA, Ault TR, Cobb KM, Deser C, Di Lorenzo E, Mantua NJ, Miller AJ, Minobe S, Nakamura H, Schneider N, Vimont DJ, Phillips AS, Scott JD, Smith CA (2016) The Pacific decadal oscillation, revisited. *J Clim* 29:4399–4427. <https://doi.org/10.1175/JCLI-D-15-0508.1>
- Oliva M, Navarro F, Hrbáček F, Hernández A, Nývlt D, Pereira P, Ruiz-Fernández J, Trigo R (2017) Recent regional climate cooling on the Antarctic Peninsula and associated impacts on the cryosphere. *Sci Total Environ* 580:210–223. <https://doi.org/10.1016/j.scitotenv.2016.12.030>
- Park J, Mann ME (2000) Interannual temperature events and shifts in global temperature: a “Multiwavelet” correlation approach. *Earth Interact* 4:1–36. [https://doi.org/10.1175/1087-3562\(2000\)004%3c0001:ITEASI%3e2.3.CO;2](https://doi.org/10.1175/1087-3562(2000)004%3c0001:ITEASI%3e2.3.CO;2)
- Parker D, Folland C, Scaife A, Knight J, Colman A, Baines P, Dong B (2007) Decadal to multidecadal variability and the climate change background. *J Geophys Res* 112:D18115. <https://doi.org/10.1029/2007JD008411>
- Rahaman W, Chatterjee S, Ejaz T, Thamban M (2019) Increased influence of ENSO on Antarctic temperature since the Industrial Era. *Sci Rep* 9:6006. <https://doi.org/10.1038/s41598-019-42499-x>
- Raphael MN (2004) A zonal wave 3 index for the Southern Hemisphere. *Geophys Res Lett* 31:L23212. <https://doi.org/10.1029/2004GL020365>
- Rasmusson EM, Carpenter TH (1982) Variations in tropical sea surface temperature and surface wind fields associated with the Southern Oscillation/El Niño. *Mon Weather Rev* 110:354–384. [https://doi.org/10.1175/1520-0493\(1982\)110%3c0354:VITSST%3e2.0.CO;2](https://doi.org/10.1175/1520-0493(1982)110%3c0354:VITSST%3e2.0.CO;2)
- Reboita MS, Ambrizzi T, Silva BA, Pinheiro RF, da Rocha RP (2019) The South Atlantic subtropical anticyclone: present and future climate. *Front Earth Sci* 7:8. <https://doi.org/10.3389/feart.2019.00008>
- Schlesinger ME, Ramankutty N (1994) An oscillation in the global climate system of period 65–70 years. *Nature* 367:723–726. <https://doi.org/10.1038/367723a0>
- Spensberger C, Reeder MJ, Spengler T, Patterson M (2020) The connection between the Southern Annular mode and a feature-based perspective on Southern Hemisphere midlatitude winter variability. *J Clim* 33:115–129. <https://doi.org/10.1175/JCLI-D-19-0224.1>
- Stastna V (2010) Spatio-temporal changes in surface air temperature in the region of the northern Antarctic Peninsula and South Shetland Islands during 1950–2003. *Polar Sci* 4:18–33. <https://doi.org/10.1016/j.polar.2010.02.001>
- Sutton RT, Hodson DLR (2005) Atlantic Ocean forcing of North American and European summer climate. *Science* 309:115–118. <https://doi.org/10.1126/science.1109496>
- Torrence C, Compo GP (1998) A practical guide to wavelet analysis. *Bull Amer Meteorol Soc* 79:61–78. [https://doi.org/10.1175/1520-0477\(1998\)079%3c0061:APGTWA%3e2.0.CO;2](https://doi.org/10.1175/1520-0477(1998)079%3c0061:APGTWA%3e2.0.CO;2)
- Trenberth KE, Caron JM, Stepaniak DP, Worley S (2002) Evolution of El Niño–Southern Oscillation and global atmospheric surface temperatures. *J Geophys Res* 107:4065. <https://doi.org/10.1029/2000JD000298>
- Turner J (2004) The El Niño–Southern Oscillation and Antarctica. *Int J Climatol* 24:1–31. <https://doi.org/10.1002/joc.965>
- Turner J, Colwell SR, Marshall GJ, Lachlan-Cope TA, Carleton AM, Jones PD, Lagun V, Reid PA, Iagovkina S (2004) The SCAR READER project: toward a high-quality database of mean Antarctic meteorological observations. *J Clim* 17:2890–2898. [https://doi.org/10.1175/1520-0442\(2004\)017%3c2890:TSRPTA%3e2.0.CO;2](https://doi.org/10.1175/1520-0442(2004)017%3c2890:TSRPTA%3e2.0.CO;2)
- Turner J, Colwell SR, Marshall GJ, Lachlan-Cope TA, Carleton AM, Jones PD, Lagun V, Reid PA, Iagovkina S (2005) Antarctic climate change during the last 50 years. *Int J Climatol* 25:279–294. <https://doi.org/10.1002/joc.1130>
- Turner J, Lu H, White I, King JC, Phillips T, Hosking JS, Bracegirdle TJ, Marshall GJ, Mulvaney R, Deb P (2016) Absence of 21st

- century warming on Antarctic Peninsula consistent with natural variability. *Nature* 535:411–415. <https://doi.org/10.1038/nature18645>
- Turner J, Marshall GJ, Clem K, Colwell S, Phillips T, Lu H (2020) Antarctic temperature variability and change from station data. *Int J Climatol* 40:2986–3007. <https://doi.org/10.1002/joc.6378>
- van Loon H, Jenne RL (1972) The zonal harmonic standing waves in the Southern Hemisphere. *J Geophys Res* 77:992–1003. <https://doi.org/10.1029/JC077i006p00992>
- Vaughan DG, Marshall GJ, Connolley WM, Parkinson C, Mulvaney R, Hodgson DA, King JC, Pudsey CJ, Turner J (2003) Recent rapid regional climate warming on the Antarctic Peninsula. *Clim Change* 60:243–274. <https://doi.org/10.1023/A:1026021217991>
- Venaille A, Sommer JL, Molines JM, Barnier B (2011) Stochastic variability of oceanic flows above topography anomalies. *Geophys Res Lett* 38:L16611. <https://doi.org/10.1029/2011GL048401>
- Venegas SA (2003) The Antarctic circumpolar wave: a combination of two signals? *J Clim* 16:2509–2525. [https://doi.org/10.1175/1520-0442\(2003\)016%3c2509:TACWAC%3e2.0.CO;2](https://doi.org/10.1175/1520-0442(2003)016%3c2509:TACWAC%3e2.0.CO;2)
- Venegas SA, Mysak LA, Straub DN (1997) Atmosphere–ocean coupled variability in the South Atlantic. *J Clim* 10:2904–2920. [https://doi.org/10.1175/1520-0442\(1997\)010%3c2904:AOCVIT%3e2.0.CO;2](https://doi.org/10.1175/1520-0442(1997)010%3c2904:AOCVIT%3e2.0.CO;2)
- Verdy A, Marshall J, Czaja A (2006) Sea surface temperature variability along the path of the Antarctic Circumpolar Current. *J Phys Oceanogr* 36:1317–1331. <https://doi.org/10.1175/JPO2913.1>
- Wallace JM (1983) The climatological mean stationary waves: observational evidence. In: Hoskins BJ, Pearce RP (eds) *Large-scale dynamical processes in the atmosphere*. Academic Press, New York, pp 27–52
- Wang X, Giannakis D, Slawinska J (2019) The Antarctic circumpolar wave and its seasonality: intrinsic travelling modes and El Niño–Southern Oscillation teleconnections. *Int J Climatol* 39:1026–1040. <https://doi.org/10.1002/joc.5860>
- White WB, Tourre YM (2003) Global SST/SLP waves during the 20th century. *Geophys Res Lett* 30:1651. <https://doi.org/10.1029/2003GL017055>
- White WB, Gloersen P, Simmonds I (2004) Tropospheric response in the Antarctic circumpolar wave along the sea ice-edge around Antarctica. *J Clim* 17:2765–2779. [https://doi.org/10.1175/1520-0442\(2004\)017%3c2765:TRITAC%3e2.0.CO;2](https://doi.org/10.1175/1520-0442(2004)017%3c2765:TRITAC%3e2.0.CO;2)
- Yang S, Webster PJ (1990) The effect of summer tropical heating on the location and intensity of the extratropical westerly jet streams. *J Geophys Res* 95:18705–18721. <https://doi.org/10.1029/JD095iD11p18705>
- Yeo SR, Kim KY (2015) Decadal changes in the Southern Hemisphere sea surface temperature in association with El Niño–Southern Oscillation and Southern Annular Mode. *Clim Dyn* 45:3227–3242. <https://doi.org/10.1007/s00382-015-2535-z>
- Yu JY, Paek H, Saltzman ES, Lee T (2015) The early 1990s change in ENSO–PSA–SAM relationships and its impact on Southern Hemisphere climate. *J Clim* 28:9393–9408. <https://doi.org/10.1175/JCLI-D-15-0335.1>
- Yuan X, Yonekura E (2011) Decadal variability in the Southern Hemisphere. *J Geophys Res* 116:D19115. <https://doi.org/10.1029/2011JD015673>
- Zazulie N, Rusticucci M, Solomon S (2010) Changes in climate at high southern latitudes: a unique daily record at Orcadas spanning 1903–2008. *J Clim* 23:189–196. <https://doi.org/10.1175/2009JCLI3074.1>
- Zitto ME, Barrucand MG, Piotrkowski R, Canziani PO (2016) 110 years of temperature observations at Orcadas Antarctic Station: multidecadal variability. *Int J Climatol* 36:809–823. <https://doi.org/10.1002/joc.4384>

**Publisher's Note** Springer Nature remains neutral with regard to jurisdictional claims in published maps and institutional affiliations.